International Journal of Power and Energy Systems, Vol. 42, No. 10, 2022
An Open Access Paper

PFoPID CONTROL DESIGN OF GRID-CONNECTED PV INVERTER FOR MPPT USING HYBRID ALGORITHM

Thomas Thangam* and K. Muthuvel*

Abstract

This paper aims to model a novel "passive fractional-order proportional-integral-derivative (PFoPID) controller" for photovoltaic (PV) inverter *via* reshaping energy, in such a way that the MPPT is attained through P&O system under diverse atmospheric states. Depending on passivity concept, storage, related to the DC-link current and DC-link voltage, in addition to q-axis current is initially build-up for a PV system, where every variable will be examined systematically when the advantageous terms are retained carefully so as to exploit the features of PV system. Here, the residual energy is reshaped by the FoPID control model, where the control constraints are optimally tuned by a new hybrid algorithm, which hybrids the concept of Cat Swarm Optimization (CSO) and Firefly Algorithm (FF), so that a finest controlling performance could be attained. As both the concepts of FF and CSO are included, the adopted model is known as Combined FF-CSO scheme (CFF-CSO).

Key Words

MPPT, energy efficiency, P&O system, irradiance and temperature, voltage

1. Introduction

Because of several ecological and cost-effective reasons, there is a rising awareness in the exploitation of renewable energy sources (RESs) [12], [13], [14]. The power systems require to be extended both vertically and horizontally [15], [16]. One method, which might offer a solution for this crisis, is the microgrid (MG), which consists of loads, storages, and distributed generators. The MG could be functioned as (1) islanded, (2) transition, and (3) grid-connected. A well-known type of RESs is PV [4], [5]. The PV thermal greenhouse system helps in the high production of biogas [6], [7], [8]. It is necessary to obtain the maximum solar power, which could be attained by functioning the PV system at "unity power factor" and by controlling the active power, known as the maximum power point tracking (MPPT) [9], [10], [11]. An MPPT system alters the operational points and it also permits PV modules to distribute the highest power [17], [18]. Nowadays, considerable developments were made in MPPT in terms of solar PV. Grid-coupled PV systems usually make use of two phases to offer the required amount of solar power to the grid. The initial phase is deployed for increasing the PV array [21], [22] voltage and it also tempts to follow the maximum solar power. Accordingly, the second phase transfers this DC power into AC power. There were highly developed attempts and extensive analysis to increase the PV throughputs [23] that are mainly concerned with improving the effectiveness of solar cell. However, the model has specific limitations, chiefly because of the substantial shortages of silicon.

In general, several MPPT [19] approaches have been deployed to regulate the output power of PV systems dynamically under the deviation of temperature and solar irradiation, such as INC, P&O, hill-climbing [20], genetic algorithm, and Grey wolf optimization. In addition, grouped grey wolf optimizer (GGWO) introduced in [1] improves the control performance and it also offers better feasibility. However, it needs more consideration on time delay. Fractional order control based incremental conductance (FOINC)-MPPT algorithm was exploited in [2] that does not fall under stability regions and it also offers high speed of tracking. In addition, PSO approach was deployed in [3] that computes the errors and it also found to be more robust. Anyhow, it needs consideration on membership functions. Likewise, reinforcement learning-based maximum power point tracking (RLMPPT) scheme was exploited in [4], which offers speedy response and does not need prior knowledge. However, it needs to be deployed in wind generator fields. In addition, microgrid-connected PV (MCPV) model was employed in [5], which offers stable operation of MG and it is simple and efficient; however, it needs consideration on tuning process. Based on the above

* Reserach Scholar, Department of Electrical and Electronics Engineering Noorul Islam Centre for Higher Education, Thuckalay, Kumaracoil, 629180, Tamil Nadu; e-mail: thomasthangam@gmail.com
** Assistant Professor, Department of Electrical and Electronics Engineering Noorul Islam Centre for Higher Education, Thuckalay, Kumaracoil, 629180, Tamil Nadu; e-mail: anusharabhakaran542@gmail.com
Corresponding author: Thomas Thangam
Recommended by Prof. Ikhlaq Hussain
(DOI: 10.2316/J.2022.203-0232)

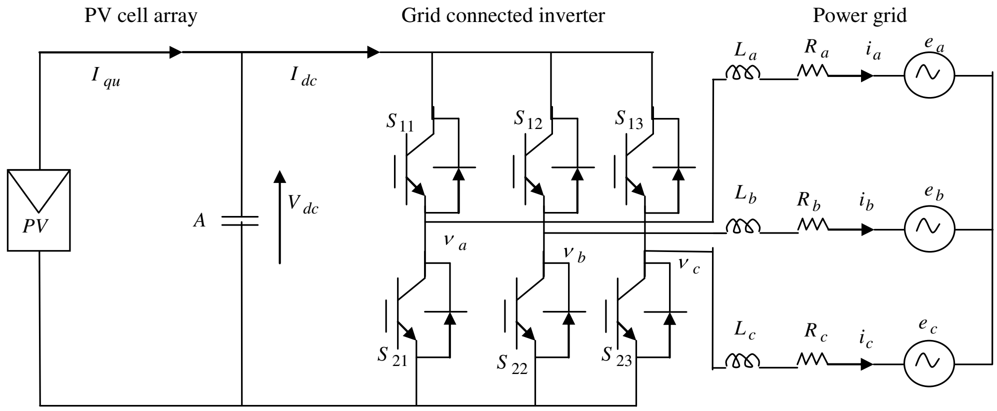

Figure 1. Representation of the three-phase two-level PV inverter.

discussion, the major contribution of this paper is depicted below.

1. This paper intends to present a novel PFoPID controller by reshaping the energy, by which MPPT is obtained *via* the P&O system under varied atmospheric conditions.
2. As per the passivity concept, a storage function related to "DC-link current and voltage" is constructed primarily for the PV system, and thus, the physical features of each variable are examined systematically for exploiting the entire necessary features of PV system.
3. Accordingly, the residual storage energy is reshaped by FoPID control model, in which the controlling constraints are optimally tuned by a CFF-CSO approach.

The overall organization of the work is as follows: Section 2 portrays the modelling of grid-connected PV inverter. Section 3 presents the preliminaries: short description. Section 4 describes the optimal parameter tuning: proposed hybrid algorithm (FF+CSO). Section 5 portrays the experimental outcomes, and this paper is concluded in Section 6.

2. System Model of MG-Connected PV Inverter

Figure 1 shows the arrangement of a single-phase PV inverter that comprises of a three-phase two-level inverter, a DC-link capacitor, three-phase power grid, and a PV array [27].

M_q and M_s indicate as the count of PV cells in parallel and series, respectively. In addition, the association among the output voltage and current is given by (1), in which I_{qu} denotes PV output current, I_{qh} denotes cell's photocurrent, B signifies p–n junction ideality factor, K denotes Boltzman's constant, C_c denotes cell's absolute working temperature, p indicates charge of electron, I_s denotes reverse saturation current of cell, and V_{dc} and I_{qu} denote PV output voltage and current, respectively, and R_s denotes cell series resistance. I_{qh} is given by (2). In addition, I_s varies in terms of temperature as per (3):

$$I_{qu} = M_q I_{qh} - M_q I_s \left(\exp\left[\frac{p}{BKC_c} \left(\frac{V_{dc}}{M_s} + \frac{I_{qu} R_s}{M_q} \right) \right] - 1 \right) \quad (1)$$

$$I_{qh} = \left[I_{sc} + K_i \left(C_c - C_{ref} \right) \right] \frac{s}{1{,}000} \quad (2)$$

$$I_s = I_{RS} \left[\frac{C_c}{C_{ref}} \right]^3 \exp\left[\frac{pF_g}{BK} \left(\frac{1}{C_{ref}} - \frac{1}{C_c} \right) \right]. \quad (3)$$

Accordingly, a PV array of 30 panels is deployed in series, whereas every module includes 36 cells in series [26], respectively:

Equation (4) shows the dynamics of three-phase two-level PV inverter in dq frame, in which e_d, e_p, i_d, i_p, u_d, u_p indicate the dq-axis elements of PV inverter grid voltage, current, and output voltage, respectively. R and L signify the corresponding resistance and inductance, respectively, and ω indicates the frequency AC grid [26]:

$$\begin{cases} u_d = e_d + Ri_d + L\frac{di_d}{dt} + \omega L i_p \\ u_p = e_p + Ri_p + L\frac{di_d}{dt} - \omega L i_d \end{cases}. \quad (4)$$

Neglect the loss of power occurring in PV inverter switches, and the balance of power association among the input side of AC and output side of DC is specified in (5), in which I_{dc} and V_{dc} are the input current and voltage of PV inverter, respectively:

$$e_d i_d + e_p i_p = V_{dc} I_{dc}. \quad (5)$$

The DC side's dynamics is attained by deploying "Kirchhoff's current law", as shown in (6), in which

A denotes the capacitance of DC bus:

$$A\frac{dV_{dc}}{dt} = I_{qu} - I_{dc} = I_{qu} - \frac{e_d i_d + e_p i_p}{V_{dc}}. \quad (6)$$

In this work, the P&O approach [28] is used for tracking the MPP efficiently under speedy time-varying atmospheric conditions.

3. Preliminaries: Short Description

3.1 Fo-PID Control

"Fractional-order calculus" is an overview of differentiation and integration and (7) shows the formulation of the basic operator ${}_{\alpha}T_t^{\alpha}$, in which t and a indicate upper and lower limits, respectively, whereas $\alpha \in \Re$ denotes the order of operation [29]:

$$ {}_{\alpha}T_t^{\alpha} = \begin{cases} \frac{d^{\alpha}}{dt^{\alpha}}, & \alpha > 0 \\ 1, & \alpha = 0 \\ \int_a^t (d\tau)^{-\alpha} & \alpha < 0 \end{cases} . \tag{7} $$

In this work, RL description is exploited with Gamma function $\Gamma(.)$, which is shown in (8), in which n denotes the 1st integer that is greater than operation order α, *e.g.*, $n-1 \leq \alpha < n$. In addition, the RL description for FoPID is given in (8):

$$ {}_{\alpha}T_t^{\alpha} f(t) = \frac{1}{\Gamma(n-\alpha)} \frac{d^n}{dt^n} \int_a^t \frac{f(\tau)}{(t-\tau)^{\alpha-n+1}} d\tau \tag{8} $$

$$ {}_{\alpha}T_t^{\alpha} f(t) = \frac{1}{\Gamma(\alpha)} \int_a^t (t-\tau)^{\alpha-1} f(\tau)\ d\tau. \tag{9} $$

The Laplace transformation of (8) is given in (10), in which $\ell\{.\}$ denotes the Laplace operator:

$$ \int_0^{\alpha} {}_0T_t^{\alpha} f(t) e^{-st} dt = s^{\alpha} \ell\{f(t)\} - \sum_{K=0}^{n-1} e^K {}_0T_t^{\alpha-K-1} f(t)|_{t=0} . \tag{10} $$

Equation (11) specifies the transfer function of FoPID control, $G(s)$, in which k_T k_I and k_q are the derivative, integral, and proportional gain, respectively:

$$ G(s) = k_q + \frac{k_I}{s^{\lambda}} + k_T s^{\mu}. \tag{11} $$

Moreover, μ and λ indicate the fractional differentiator order and fractional integrator order, respectively.

3.2 Passivity-Oriented Controlling and Energy Reshaping

The PBC is operated with a minimal storage function at the desired point of equilibrium. In addition, PBC tends to remodel the energy of the system and it further attempts to allocate an energy function, which is equivalent to the variation among the supplied energy and system's energy.

Equation (12) demonstrates the equation for energy balancing, which $d(t)$ specifies a non-negative function and $U(t)$ denotes the storage function:

$$ \underset{Stored}{U[y(t)] - U[y(0)]} = \underset{Supplied}{\int_0^t v^C(s)\, x(s)} - \underset{Dissipated}{d(t)} . \tag{12} $$

3.3 PFoPID Controller for MPPT

Controller Model: Portray the state vector as $y = (y_1, y_2, y_3)^C = (i_d, i_p, V_{dc})^C$, input $v = (v_1, v_2)^C = (u_d, u_p)^C$ and output $x = (x_1, x_2)^C = (i_p, V_{dc})^C$. Thus, (4) and (6) are mentioned, as given in the following equation [1]:

$$ \dot{y} = \begin{pmatrix} -\frac{R}{L}y_1 - \omega y_2 - \frac{e_d}{L} \\ -\frac{R}{L}y_2 + \omega y_1 - \frac{e_p}{L} \\ \frac{I_{qu}}{A}{}_1 - \frac{e_d y_1 + e_p y_2}{A y_3} \end{pmatrix} + \begin{pmatrix} \frac{1}{L} & 0 \\ 0 & \frac{1}{L} \\ 0 & 0 \end{pmatrix} v. \tag{13} $$

Describe the tracking error $e = (e_1, e_2)^C = \left[i_p,\ i_p^*,\ V_{dc} - V_{dc}^*\right]^C$. The tracking error e is differentiated till the control input v becomes precise, and thus, (14) is formed, in which $f_1(y)$ and $f_2(y)$ are given in (15) and (16):

$$ \begin{bmatrix} \dot{e}_1 \\ \ddot{e}_2 \end{bmatrix} = \begin{bmatrix} f_1(y) \\ f_2(y) \end{bmatrix} + A(y) \begin{bmatrix} v_1 \\ v_2 \end{bmatrix} - \begin{bmatrix} \dot{i}_p^* \\ \ddot{V}_{dc}^* \end{bmatrix} \tag{14} $$

$$ f_1(y) = -\frac{R}{L} i_p + \omega i_d - \frac{e_p}{L} \tag{15} $$

$$ f_2(y) = \frac{i_{qu}}{A} - \frac{e_d\left(-\frac{R}{L}i_p - \omega i_p - \frac{e_p}{L}\right) + e_p\left(-\frac{R}{L}i_p + \omega i_d - \frac{e_p}{L}\right)}{AV_{dc}} - \frac{(e_d i_d + e_p i_p)}{A^2 V_{dc}^2} I_{qu} + \frac{(e_d i_d + e_p i_p)^2}{A^2 V_{dc}^3} \tag{16} $$

$$ \dot{U}(i_p, V_{dc}, I_{dc}) = -\frac{1}{AR_{dc}}\left(\dot{V}_{dc} - \dot{V}_{dc}^*\right)^2 - \frac{R}{L}\left(i_p - i_p^*\right)^2 - \left(\dot{V}_{dc} - \dot{V}_{dc}^*\right)^2 v_1 - \frac{i_p - i_p^*}{L} v_2. \tag{17} $$

In (17), $R_{dc} = \frac{V_{dc}^2}{e_d i_d + e_p i_p}$ indicates a virtual resistor with DC-link capacitor, and v_1 and v_2 are the inputs being modelled in the FoPID control form [1].

4. Optimal Parameter Tuning: Proposed Hybrid Algorithm (FF+CSO)

4.1 Objective Function and Solution Encoding

The PFoPID constraints in (21) are tuned optimally *via* CFF-CSO model, such that optimal control should be attained. Here, the objective function intends to minimize $F(y)$, which is described in (23). The solution encoding of the presented work is given in Fig. 2, where k_Q, k_I, k_D, λ, μ are given as input:

$$ Minimize\ F(y) = Mean\left[Mean\left|\left(V_{dc_{ref}} - V_{dc}\right)\right|\right]. \tag{18} $$

4.2 Proposed Algorithm: CFF-CSO

Fireflies are charismatic insects [24]. The flashing light of fireflies is their major feature that comprises of two basic

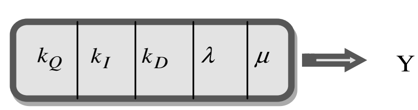

Figure 2. Solution encoding.

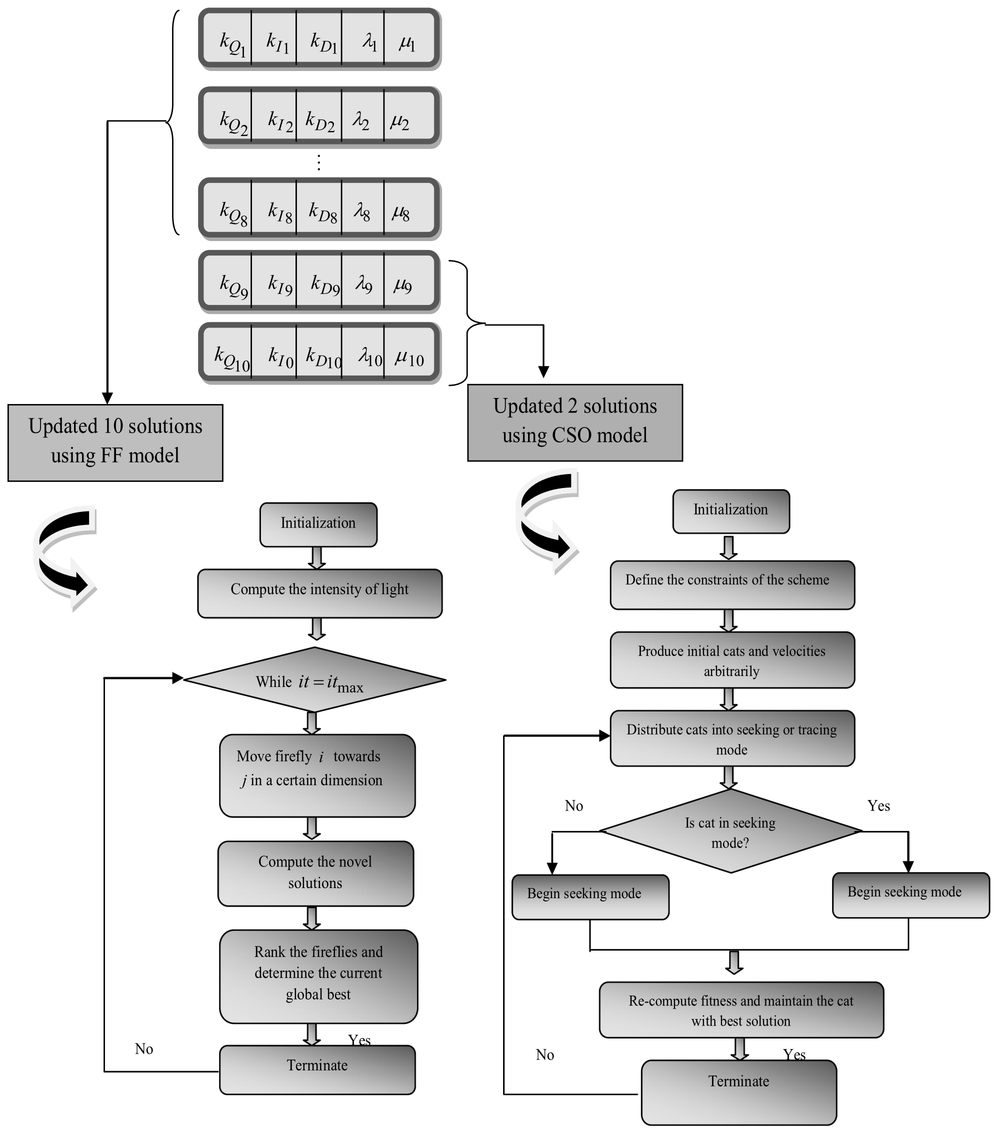

Figure 3. Flowchart of the proposed model.

characteristics, such as attraction and warning of hunters. The CSO model mimics the food searching behaviour of cats [25]. Moreover, CSO cat population are generated and are dispersed randomly, and accordingly, every cat indicates a solution [31]. This population is separated into two groups. The cats in 1st group rest observe its surroundings, which are said to be the seeking mode, whereas the cats in 2nd group begin to move and chase its prey and it is known as tracing mode. For the attainment of optimal control performance, this paper aims to present a new hybrid scheme that hybrids the concept of FF and CSO, respectively. Even though, the conventional FF algorithm poses various advantages including accurate approximations; it also seems to be little constricting by means of convergence rate. Similarly, CSO needs to be improved for overcoming the local optima issue. Hence, it is planned to mingle both the concepts in a certain way that obviously solve the optimization problems with better convergence:

The procedure of the adopted scheme is: usually, the population size is user-defined. In the present model, the population size is fixed as ten. Among the ten solutions, the eight solutions are updated using the FF model, whereas the remaining two solutions are updated using the CSO model, *i.e.,* at 4:1 ratio, where the largest proportion gets updated using FF and the smallest proportion gets updated using CSO. As the concepts of both FF and CSO are included, the presented scheme is named CFF-CSO model. The flowchart representation of the adopted scheme is given in Fig. 3. The primary process of the FF model is initialization. Here, the light absorption is computed by the deployment of the light absorption coefficient. Besides, it check for the condition of whether the iteration $it = it_{\max}$ is $it_{\max}$. Move fireflies i in the direction of j in a certain dimension. Then, the novel solution is computed. Finally, the current global best solution is ranked and established. If the conditions are satisfied, stop the process, otherwise continue with steps 3. At first, the cat population is

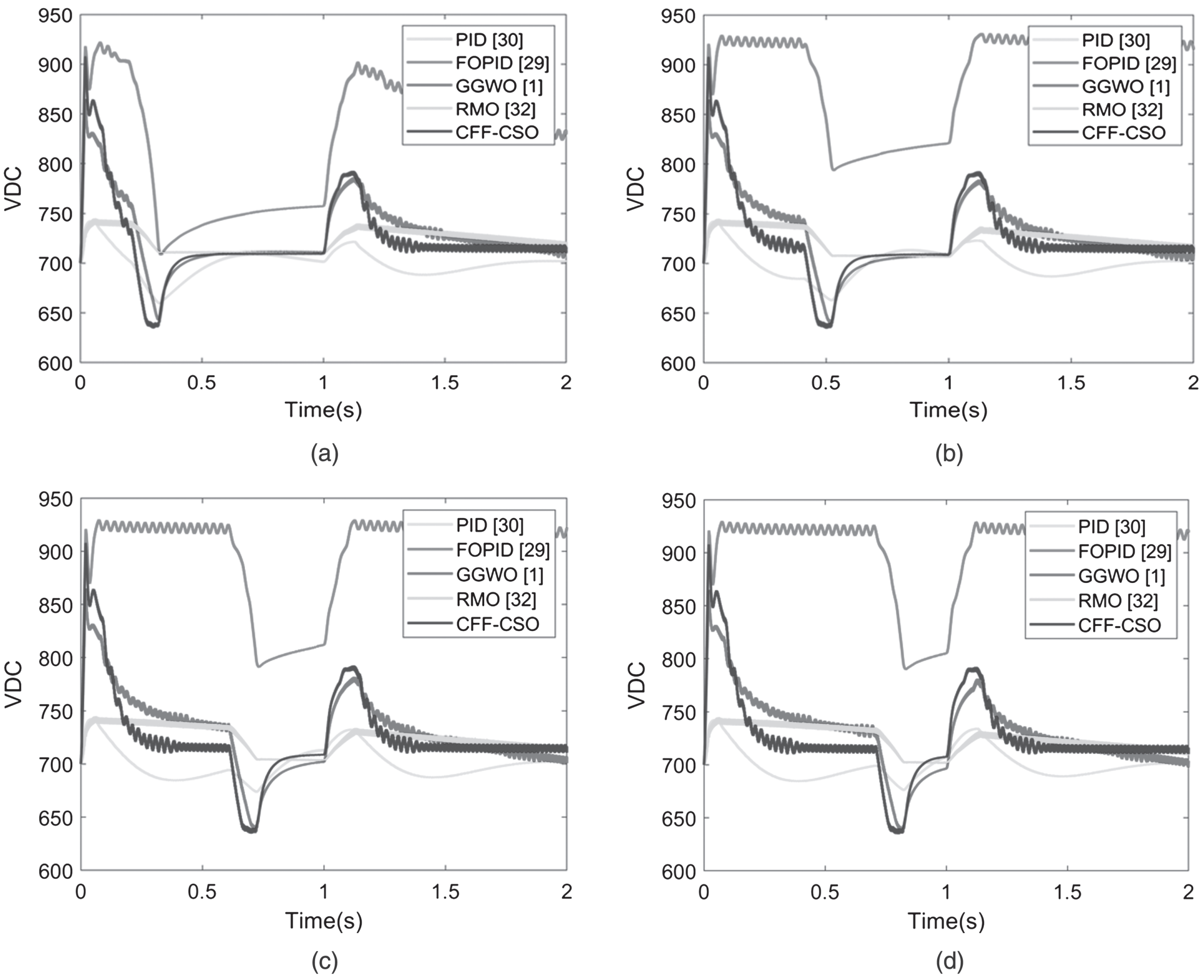

Figure 4. Voltage analysis of the proposed and traditional controllers by varying irradiance and temperature levels (a) (0.2, 20), (b) (0.4, 40), (c) (0.6, 60), and (d) (0.7, 70), respectively.

initialized and the constraints of the scheme are specified. Moreover, the initial cats and velocities are produced in a random manner. Then, all cats are distributed into the seeking or tracing mode. In addition, check whether the cat is in searching or tracing mode. The fitness of every cat is computed and the one with optimal fitness is saved. The best position of the cat indicates the optimal solution attained till now. Depending upon their flags, tracing or seeking mode is allocated for the cats as specified below. If the conditions are fulfilled, finish the process, or else with continue step 4.

5. Results and Discussion

5.1 Simulation Procedure

The simulation of CFF-CSO for optimal controller performance was performed in MATLAB and the results were attained. The presented CFF-CSO scheme was evaluated over the traditional schemes, such as PID [30], FoPID [29], GGWO [1], and radial movement optimization (RMO) [32]. Here, the experimentations were carried out by varying the irradiance and temperature to four levels, namely, (0.2, 20), (0.4, 40), (0.6, 60), and (0.7, 70), concerning PV output voltage V_{dc} and voltage reference $V_{dc_{ref}}$. Moreover, the error deviation among V_{dc} and $V_{dc_{ref}}$ was also determined from the simulation outcomes.

5.2 Voltage Analysis

The output of PV voltage is described in this section by varying the irradiance and temperature to four levels, namely, (0.2, 20), (0.4, 40), (0.6, 60), and (0.7, 70), respectively. Here, the reference voltage V_{dc} is set at the range of 700. For optimal attainment of the controlling performance, the voltage of the controllers should be nearer to $V_{dc_{ref}}$ (700V). From the observed outcomes, the presented CFF-CSO-based controller is found to be nearer to the fixed target (700V) when compared over the traditional schemes. Figure 4(a) depicts the irradiance and temperature of (0.2, 20), where the presented controller is nearer to $V_{dc_{ref}}$. Likewise, for all the levels of irradiance and temperature, the adopted CFF-CSO-based controller is closer to $V_{dc_{ref}}$ of 700V which can be noted from Fig. 4(b), (c), and (d). Though the RMO [32] has less deviation from the reference voltage, it is highly insensitive to the disturbance. As per Fig. 4, disturbances are introduced at two-time instants say 0.1s and 1s. The proposed algorithm is sensitive to the disturbance and attempts to retain the reference voltage, whereas RMO [32] does not show a significant

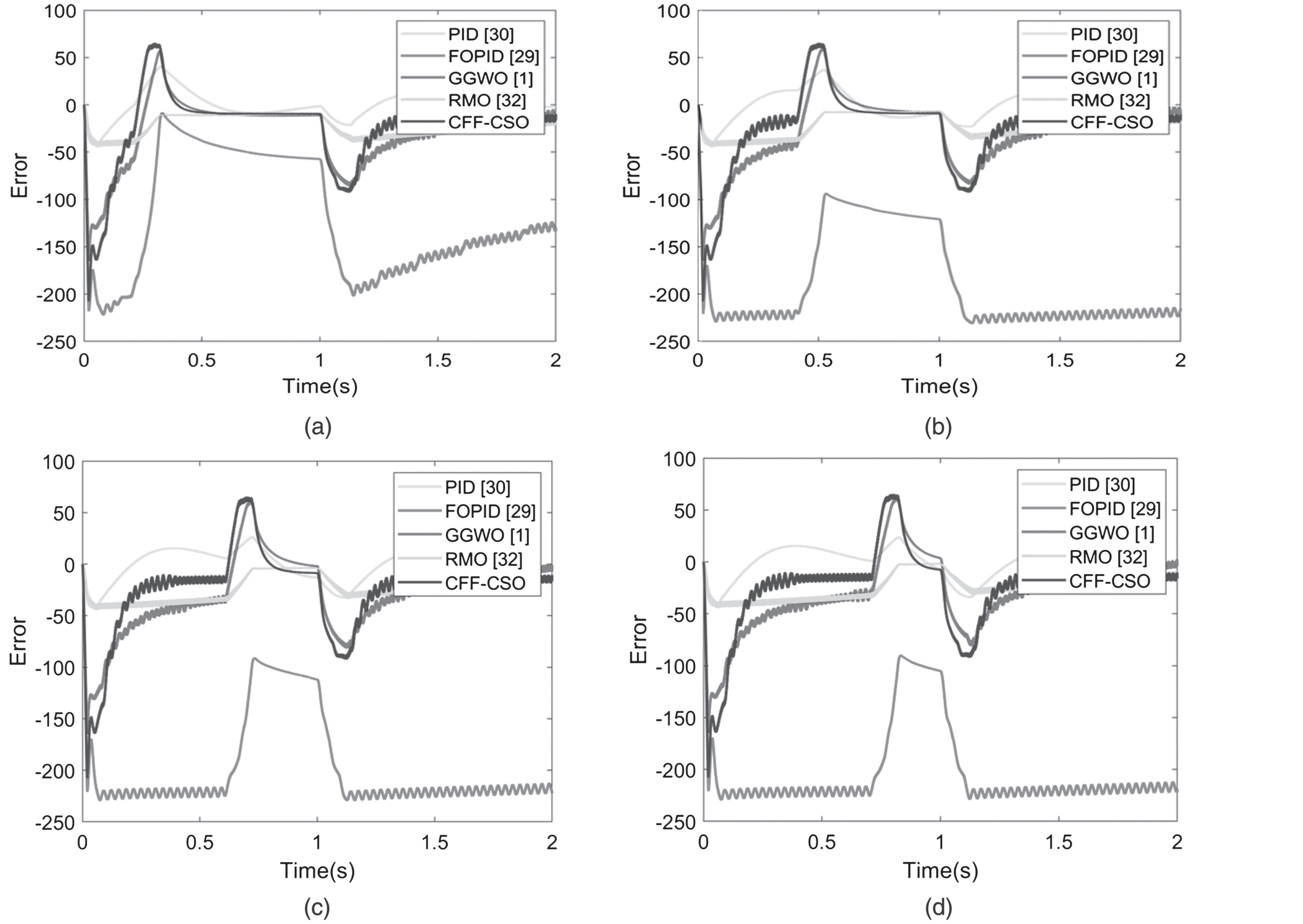

Figure 5. Voltage analysis of the proposed and traditional controllers by varying irradiance and temperature levels (a) (0.2, 20), (b) (0.4, 40), (c) (0.6, 60), and (d) (0.7, 70).

response to the disturbance. This infers that the proposed method relatively responds to the disturbance. Despite the settling performance is a factor, the trade-off between sensitivity against disturbance and settling is significant.

5.3 Voltage Error Analysis

The error among V_{dc} and voltage reference $V_{dc_{ref}}$ is specified in Fig. 5 by varying the irradiance and temperature to four levels, namely, (0.2, 20), (0.4, 40), (0.6, 60), and (0.7, 70), respectively. The error should be minimal between V_{dc} and $V_{dc_{ref}}$ for better controlling performance. From Fig. 5(a), the error of the adopted CFF-CSO-based controller is nearer to zero, whereas the other conventional schemes pose error between V_{dc} and $V_{dc_{ref}}$. Thus, for all varying levels of irradiance and temperature, the presented scheme has attained a value nearer to zero, thus showing a minimal error. Thus, the betterment of the adopted CFF-CSO-based controller is proved over other conventional models.

5.4 Optimization Analysis

The optimal values attained by the presented CFF-CSO and traditional schemes are given in Table 1.

Table 1
Optimal Values Attained by the Proposed and Conventional Models

Objectives	GGWO [1]	RMO [32]	CFF-CSO
k_Q	10.927	20	18.354
k_I	12.93	16.748	10.222
k_D	17.362	20	18.746
λ	1.8446	1	0.1
μ	0.4038	1	0.11568

5.5 Performance Analysis on MPPT of the Proposed Method

This section discusses about the performance analysis on MPPT of the proposed CFF-CSO method, which is illustrated in Fig. 6. As observed in Fig. 6, it can be noticed that the proposed MPPT shows less oscillation in steady state and faster converging speed when compared with conventional PID, FoPID, GGWO, and RMO methods. Thus, the superiority of the proposed MPPT method over conventional methods has been confirmed.

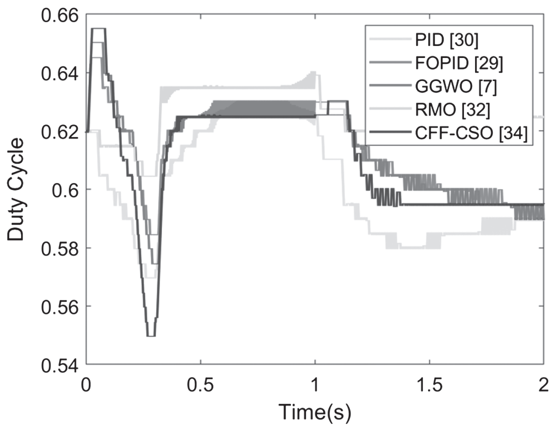

Figure 6. Experimental analysis of the proposed MPPT and traditional methods.

6. Conclusion

This paper has presented a novel PFoPID controller for PV inverter by reshaping the energy, and here, the MPPT was obtained *via* the P&O system under varied states. The residual energy of the storage function was reshaped by the FoPID control model, in which the controlling constraints are optimally tuned by a CFF-CSO approach. Finally, the performance of the implemented approach was compared over other traditional schemes to confirm the efficiency of the adopted technique. From the observed outcomes, the presented CFF-CSO-based controller was found to be nearer to the fixed target (700V) when compared to the traditional schemes. Likewise, the error of the adopted CFF-CSO-based controller is nearer to zero, whereas the other conventional schemes poses error between V_{dc} and $V_{dc_{ref}}$.

References

[1] B. Yang, T. Yu, H. Shu, D. Zhu, L. Jiang, Energy reshaping based passive fractional-order PID control design and implementation of a grid-connected PV inverter for MPPT using grouped grey wolf optimizer, *Solar Energy*, *170*, 2018, 31–46 .

[2] M. Al-Dhaifallah, A.M. Nassef, H. Rezk, K.S. Nisar, Optimal parameter design of fractional order control based INC-MPPT for PV system, *Solar Energy*, 159, 2018, 650–664.

[3] Y.-Y. Hong, A.A. Beltran, and A.C. Paglinawan, A robust design of maximum power point tracking using Taguchi method for stand-alone PV system, *Applied Energy*, *211*, 2018, 50–63.

[4] P. Kofinas, S. Doltsinis, A.I. Dounis, and G.A. Vouros, A reinforcement learning approach for MPPT control method of photovoltaic sources, *Renewable Energy*, *108*, 2017, 461–473.

[5] A. Elrayyah, Y. Sozer, and M. Elbuluk, Microgrid-connected PV-based sources: A novel autonomous control method for maintaining maximum power, *IEEE Industry Applications Magazine*, *21*(2), 2015, 19–29.

[6] Y.-T. Chen, Y.-C. Jhang, and R.-H. Liang, A fuzzy-logic based auto-scaling variable step-size MPPT method for PV systems, *Solar Energy*, *126*, 2016, 53–63.

[7] H. Yatimi and E. Aroudam, Assessment and control of a photovoltaic energy storage system based on the robust sliding mode MPPT controller, *Solar Energy*, *139*, 2016, 557–568.

[8] S. Saravanan and N.R. Babu, RBFN based MPPT algorithm for PV system with high step up converter, *Energy Conversion and Management*, *122*, 2016, 239–251.

[9] Md. F. Ansari, S. Chatterji, and A. Iqbal, A fuzzy logic control scheme for a solar photovoltaic system for a maximum power point tracker, *International Journal of Sustainable Energy*, *29*(4), 2010, 245–255.

[10] C.Y. Yang, C.Y. Hsieh, F.K. Feng, and K.H. Chen, Highly Efficient Analog Maximum Power Point Tracking (AMPPT) in a photovoltaic system, *IEEE Transactions on Circuits and Systems I: Regular Papers*, *59*(7), 2012, 1546–1556.

[11] A.K. Abdelsalam, A.M. Massoud, S. Ahmed, and P.N. Enjeti, High-performance adaptive perturb and observe MPPT technique for photovoltaic-based MGs, *IEEE Transactions on Power Electronics*, *26*(4), 2011, 1010–1021.

[12] T.F. Wu, C.H. Chang, L.C. Lin, and C.L. Kuo, Power loss comparison of single- and two-stage grid-connected photovoltaic systems, *IEEE Transactions on Energy Conversion*, *26*(2), 2011, 707–715.

[13] A.H. El Khateb, N. A. Rahim, and J. Selvaraj, Type-2 fuzzy logic approach of a maximum power point tracking employing SEPIC converter for photovoltaic system, *Journal of Clean Energy Technologies*, *1*(1), 2013.

[14] M. Seyedmahmoudian *et al.*, Simulation and hardware implementation of new maximum power point tracking technique for partially shaded PV system using hybrid DEPSO method, *IEEE Transactions on Sustainable Energy*, *6*(3), 2015, 850–862.

[15] B. N. Alajmi, K. H. Ahmed, S. J. Finney, and B. W. Williams, Fuzzy-logic-control approach of a modified hill-climbing method for maximum power point in MG standalone photovoltaic system, *IEEE Transactions on Power Electronics*, *26*(4), 2011, 1022–1030.

[16] M. Mohammadi and M. Nafar, Fuzzy sliding-mode based control (FSMC) approach of hybrid micro-grid in power distribution systems, *International Journal of Electrical Power & Energy Systems*, *51*, 2013, 232–242.

[17] A.I. Dounis, P. Kofinas, G. Papadakis, and C. Alafodimos, A direct adaptive neural control for maximum power point tracking of photovoltaic system, *Solar Energy*, *115*, 2015, 145–165.

[18] S. Li, A variable-weather-parameter MPPT control strategy based on MPPT constraint conditions of PV system with inverter, *Energy Conversion and Management*, *197*, 2019, Article 111873.

[19] S.L. Brunton, C.W. Rowley, S.R. Kulkarni, and C. Clarkson, Maximum power point tracking for photovoltaic optimization using ripple-based extremum seeking control, *IEEE Transactions on Power Electronics*, *25*(10), 2010, 2531–2540.

[20] Y. Du, D.D.-C. Lu, G. James, and D.J. Cornforth, Modeling and analysis of current harmonic distortion from grid connected PV inverters under different operating conditions, *Solar Energy*, *94*, 2013, 182–194.

[21] B. Boukezata, J.-P. Gaubert, A. Chaoui, and M. Hachemi, Predictive current control in multifunctional grid connected inverter interfaced by PV system, *Solar Energy*, *139*, 2016, 130–141.

[22] G.J. Kish, J.J. Lee, and P.W. Lehn, Modelling and control of photovoltaic panels utilising the incremental conductance method for maximum power point tracking, *IET Renewable Power Generation*, *6*(4), 2012, 259–266.

[23] S. Jiang, D. Cao, Y. Li, and F.Z. Peng, Grid-connected boost-half-bridge photovoltaic microinverter system using repetitive current control and maximum power point tracking, *IEEE Transactions on Power Electronics*, *27*(11), 2012, 4711–4722.

[24] I. Fister, I. Fister, X.-S. Yang, and J. Brest, A comprehensive review of firefly algorithms, *Swarm and Evolutionary Computation*, *13*, 2013, 34–46.

[25] S.-C. Chu, P.-w. Tsai, and J.-S. Pan, *Cat Swarm Optimization*, Conference Paper in Lecture Notes in Computer Science, 12 March 2014.

[26] D. Lalili, A. Mellit, N. Lourci, B. Medjahed, and E.M. Berkouk, Input output feedback linearization control and variable step size MPPT algorithm of a grid-connected photovoltaic inverter, *Renewable Energy, 36*, 2011, 3282–3291.

[27] R. Kadri, J.P. Gaubert, and G. Champenois, An improved maximum power point tracking for photovoltaic grid-connected inverter based on voltage-oriented control, *IEEE Transactions on Industrial Electronics*, *58*(1), 2011, 66–75.

[28] R. Alik and J. Awang, Modified Perturb and Observe (P&O) with checking algorithm under various solar irradiation, *Solar Energy*, *148*, 2017, 128–139.

[29] I. Podlubny, *Fractional Differential Equations.* Academic Press, New York, 1999.

[30] U.E. Ayten, E. Yuce, and S. Minaei, A voltage-mode PID controller using a single CFOA and only grounded capacitors, *Microelectronics Journal*, *81*, 2018, 84–93.

[31] L. Pappula and D. Ghosh, Cat swarm optimization with normal mutation for fast convergence of multimodal functions, *Applied Soft Computing*, *66*, 2018, 473–491.

[32] M. Vanithasri, R. Balamurugan, and L. Lakshminarasimman, Radial movement optimization (RMO) technique for solving unit commitment problem in power systems, *Journal of Electrical Systems and Information Technology*, *5*(3), 2018, 697–707.

Biographies

Thomas Thangam was born in Pudukkottai, India in 1973. Received the B.E., (EEE) degree from Government College of Engineering, Manonmaniam Sundaranar University, India in 1995 and M.E., (PED) from Alagappa Chettiar College of Engineering and Technology, Anna University, India in 2005. At present, working as a Lecturer in International Maritime College of Oman, Sohar, Sultanate of Oman. Has published two papers in national level Journals/Conferences. Field of interest includes Power electronics, Photovoltaic system, Power systems and Renewable Energy Sources. Having 21 Years in Teaching and 3 Years in Industry.

Dr. K. Muthuvel published two books, five papers in international referred Journals, five papers in international conferences, and two papers in national conferences. Received Best Paper Award at IEEE International Conference on Circuit, Power and Computing Technologies (ICCPCT 2014) held on March 2014. He has experience in teaching (12 years and 9 months) and industry (4 years 7 months).